

Title

**Selective laser sintering of high carbon steel powders studied as a  
function of carbon content**

Authors

Takayuki Nakamoto <sup>a,\*</sup>, Nobuhiko Shirakawa <sup>a</sup>, Yoshio Miyata <sup>a</sup>, Haruyuki Inui <sup>b</sup>

Affiliations and addresses

<sup>a</sup> *Technology Research Institute of Osaka Prefecture, 2-7-1 Ayumino, Izumi-shi, Osaka  
594-1157, Japan*

<sup>b</sup> *Department of Materials Science and Engineering, Kyoto University, Sakyo-ku, Kyoto  
606-8501, Japan*

**Abstract**

Optimum conditions for laser irradiation to achieve fully dense high carbon steel SLS (Selective Laser Sintering) specimens have been investigated as a function of carbon content in steel powders with the use of steel powders with different carbon contents in the range of 0.33-1.05 mass%C (corresponding to S33C, S50C, S75C and S105C in the JIS standard). Full densification is found to be easily achieved by SLS

processing for all high carbon steel powders. The energy density during the SLS process required for full densification decreases as the carbon content increases from 400 J/mm<sup>3</sup> for 0.33 and 0.50 mass%C to 267 J/mm<sup>3</sup> for 0.75 and 1.05 mass%C. This is considered to be due to the increased wettability of molten Fe-C alloys for the higher carbon contents. The values of microhardness and yield stress of fully dense SLS specimens tend to increase as the carbon content in steel powders increases. At a given carbon content, the values of microhardness and yield stress of fully dense SLS specimens tend to be higher for those produced with a lower energy input (with higher laser scan speeds and larger scan spacings).

**Keywords** Selective laser sintering (SLS); Carbon steel powder; Densification; Microstructure; Mechanical property; Rapid prototyping (RP)

\* Corresponding author:

Takayuki Nakamoto

Tel: (81)725512563

Fax: (81)725512599

e-mail : nakamoto@tri.pref.osaka.jp

Main text

## **1. Introduction**

Selective laser sintering (SLS) is one of the rapid prototyping (RP) techniques that allow producing complex three-dimensional parts rapidly from CAD (computer aided design) models by sintering successive thin layers of powder with a laser beam (Kruth et al., 2001). Especially SLS with a metallic powder is an attractive process for rapidly manufacturing molds (Abe et al., 2006; ÓDonnchadha and Tansey, 2004), dies (Abe et al., 2001) and mechanical parts (Levy et al., 2003). We have recently investigated SLS processes of low carbon (0.15 mass%) steel powder (Nakamoto et al., 2008) and clarified that complete elimination of pores is indispensable for the ductility and strength of SLS specimens and that an energy density (the total energy input per unit volume of each sintered layer) (Simchi and Pohl, 2003) greater than  $800 \text{ J/mm}^3$  is needed for full densification of the low carbon steel (with the density comparable to that of the corresponding wrought material). It is indispensable to investigate SLS processes of high carbon steels when referring to the practical importance in their applications to molds, dies and mechanical parts. Many studies have indeed been conducted on SLS processes of high carbon steels with the use of high speed steel (Simchi and

Asgharzadeh, 2004; Niu and Chang, 1998), tool steel (Otsu et al., 2005) powders and a mixture of iron and graphite powders (Murali et al., 2003; Simchi and Pohl, 2004; Rombouts et al., 2006). Many of them have concluded, however, that full densification is not achieved for high carbon steel SLS parts made with these powders, exhibiting only a density below about 94% those of the corresponding wrought materials. The imposed energy density during the SLS process is obviously insufficient for full densification of these steels. The high melting points of some carbides and graphite are considered to be one of the reasons for this when high-alloy steel powders and a mixture of iron and graphite powders are used, respectively. Of interest to note, however, is that when a mixture of iron and graphite powders are used, the density of SLS steel parts increases with the increase in the carbon content, because the wettability of molten Fe-C alloys is expected to be larger as the carbon content increases (Simchi and Pohl, 2004; Rombouts et al., 2006). This suggests that if the imposed energy density during the SLS process is sufficiently high, full densification of high carbon steel SLS parts is expected to achieve more easily as the carbon content increases. This has yet to be clarified.

In the present study, we investigate optimum conditions for laser irradiation to achieve fully dense high carbon steels by the SLS process and their sintering (pore formation) mechanisms as a function of carbon content, with the use of carbon steel

powders instead of a mixture of iron and graphite powders, with which full densification is expected to be very difficult to achieve because of difficulty in melting graphite by laser irradiation. We also investigate microstructures as well as mechanical properties of SLS steels as a function of laser irradiation condition and carbon content in steel powders.

## 2. Experimental procedure

Carbon steel powders with a mean particle size of about 30  $\mu\text{m}$  were produced by water atomization. Chemical compositions of these carbon steel powders are tabulated in Table 1. As in Table 1, the chemical compositions of the carbon steel powders containing 0.33 and 0.49 mass% carbon are equivalent to those of S33C and S50C steels in the JIS standard, while those of the carbon steel powders containing 0.76 and 1.04 mass% carbon are almost equivalent to those of SK75 and SK105, except for the Si

Table 1 Chemical composition of carbon steel powders (mass%). Numbers in ( ) indicate the carbon contents after SLS processing.

Material	C	Si	Mn	P	S
S33C	0.33 (0.31)	0.19	0.64	0.010	0.003
S50C	0.49 (0.46)	0.22	0.79	0.006	0.005
S75C	0.76 (0.71)	0.28	0.77	0.009	0.008
S105C	1.04 (0.99)	0.21	0.74	0.009	0.007

and Mn contents. The Si, Mn, P and S contents are almost identical for these four steels. These steels are thus designated respectively to S33C, S50C, S75C and S105C throughout the present paper. In the Fe-C phase diagram, the C content of S75C corresponds to the eutectoid composition, and thus S33C and S50C correspond to hypoeutectoid steels and S105C to a hypereutectoid one.

Laser sintering was conducted in a nitrogen atmosphere with an EOSINT M250 Xtended (EOS GmbH, Germany) laser sintering machine by irradiating a CO<sub>2</sub> laser with the maximal power of 240 W and the beam diameter of 0.4 mm. Cylindrical SLS specimens with 8 mm in diameter and 15 mm in height were built under various laser irradiation conditions listed in Table 2.

Density measurements were made immediately after fabrication by the Archimedean method in conformity with JIS Z 2501 (corresponding to ISO/DIS 2738). SLS specimens were first weighed in the air and then were thinly covered with paraffin wax in order to prevent the water from infiltrating into pores. Those covered specimens

Table 2 Laser irradiation conditions

Laser power	/W	200
Scan speed	/mm/s	50, 100, 150, 200
Scan spacing	/mm	0.1, 0.2, 0.3, 0.4
Layer thickness	/mm	0.05

were weighed in the air and in the water, and the volume of the specimens was calculated from the difference between the last two weights. Microstructures of SLS specimens in a cross-section parallel to the building direction were examined by optical microscopy after immersing the specimens in an etchant of 3% nital (3% HNO<sub>3</sub> in alcohol) or of hydrochloric picral. Surface morphologies of sintered specimens were examined with a scanning electron microscope (SEM). Compression tests were conducted on an Instron-type testing machine at a cross-head speed of 2 mm/min corresponding to a strain rate of  $2.8 \times 10^{-3} \text{ s}^{-1}$ . Specimens for compression tests, measuring 8 mm in diameter and 12 mm in height, were cut from a cylindrical SLS specimen with 15 mm in height. Microhardness measurements were also made with a Vickers hardness tester with a load of 4.9 N for 15 s.

### **3. Results and discussion**

#### **3.1. Density and pore distribution of SLS specimens**

Optical microstructures of SLS specimens produced with S75C powder under various laser irradiation conditions are depicted in Fig. 1. Dark areas in Fig. 1 correspond to pores. For both scan speeds (50 and 100 mm/s), pores are formed in parallel to the building direction when the scan spacing is 0.4 mm (Figs. 1(a) and (e)).

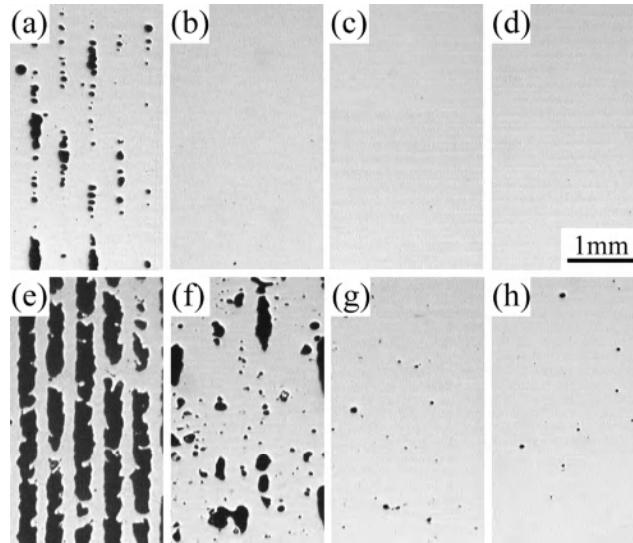


Fig. 1 Optical microstructures of SLS specimens produced with S75C steel powder under various laser irradiation conditions with the scan speed/scan spacing of (a) 50 mm/s, 0.4 mm, (b) 50 mm/s, 0.3 mm, (c) 50 mm/s, 0.2 mm, (d) 50 mm/s, 0.1 mm, (e) 100 mm/s, 0.4 mm, (f) 100 mm/s, 0.3 mm, (g) 100 mm/s, 0.2 mm and (h) 100 mm/s, 0.1 mm, respectively. Observations were made in a cross-section cut parallel to the building direction.

The volume fraction of pores drastically decreases when the scan spacing decreases from 0.4 mm (Figs. 1(a) and (e)) to 0.3 mm (Figs. 1(b) and (f)) for the scan speed of 50 mm/s, and to 0.2 mm (Figs. 1(c) and (g)) for the scan speed of 100 mm/s, as the extent of the overlapping of laser-beam scan paths becomes more significant. On the other hand, the volume fraction of pores decreases as the scan speed decreases from 100 mm/s to 50 mm/s at a given scan spacing. As a result, SLS specimens formed at the scan spacing less than 0.3 mm exhibit a microstructure free from pores at the scan speed of 50 mm/s, as shown in Figs. 1(b), (c) and (d). When the scan speed is increased above

150 mm/s, however, SLS processing was impossible to be completed even at the scan spacing of 0.1 mm. This is due to the collision of the sintered specimen with the recoating blade occurring after sintering the first few layers as a result of the formation of irregularly tall protrusions on the sintering surface (see, the details in the 3.2. section).

A similar trend is observed in the condition to produce pore-free SLS specimens (at smaller scan spacings and scan speeds) for all steel powders used. This clearly indicates that the scan spacing should be decreased well below the beam diameter (0.4 mm) and that there is a critical value of the energy density (defined as the total energy input per unit volume) for full densification, which varies with the carbon content of steels. The energy density during the SLS process required for full densification decreases as the

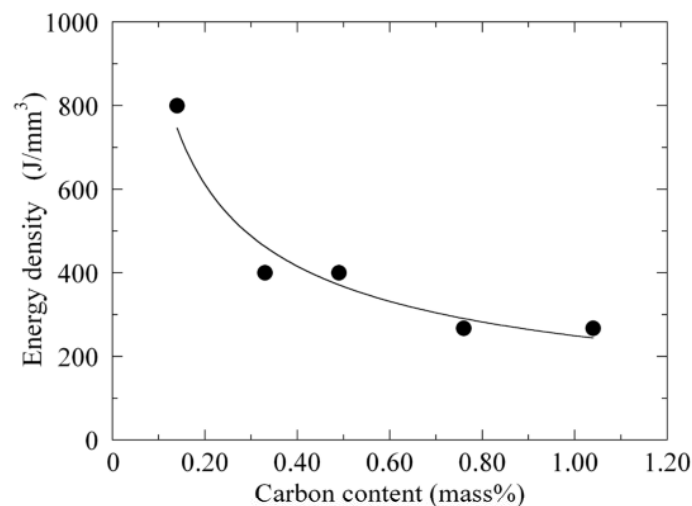


Fig. 2 Energy density required for full densification by SLS processing plotted as a function of carbon content in steel powders.

carbon content increases from  $800 \text{ J/mm}^3$  for 0.15 mass%C to  $400 \text{ J/mm}^3$  for 0.33 and 0.50 mass%C, and to  $267 \text{ J/mm}^3$  for 0.75 and 1.05 mass%C, as shown in Fig. 2. As for low carbon (0.15 mass%) steel powder, we have recently clarified that the SLS specimen is virtually free from pores when the laser irradiation condition with the laser power of 200 W, the layer thickness of 0.05 mm, the scan speed of 50 mm/s and the scan spacing of 0.1 mm, which corresponds to the energy density of  $800 \text{ J/mm}^3$ , is employed (Nakamoto et al., 2008). As tabulated in Table 1, the carbon loss due to evaporation during SLS processing is very small for fully dense SLS specimens, irrespective of carbon content. However, when the laser irradiation conditions with an energy density insufficient for full densification are employed, quite different

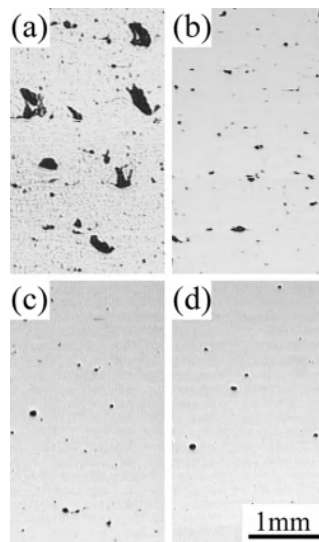


Fig. 3 Optical microstructures of SLS specimens produced with (a) S33C, (b) S50C, (c) S75C and (d) S105C steel powders at the scan speed of 100 mm/s and scan spacing of 0.2 mm. Observations were made in a cross-section cut parallel to the building direction.

densification behaviors are observed depending on carbon content of steel powders, as depicted in Fig. 3. The irradiation condition employed for Fig. 3 is the scan speed of 100 mm/s and the scan spacing of 0.2 mm, which is the same as that used to produce the almost pore-free S75C SLS specimen of Fig. 1(g). The volume fraction of pores in SLS specimens obviously increases as the carbon content in steel powders decreases from S75C (Fig. 3(c)) to S50C (Fig. 3(b)) and to S33C (Fig. 3(a)), while the volume fractions of pores in S75C and S105C SLS specimens are identically very small. A similar tendency (the higher is the carbon content, the denser the SLS specimen is) is observed for SLS specimens produced with a mixture of iron and graphite powders by Simchi and Pohl (2004). Of importance to note, however, is that the highest densities of SLS specimens produced in the present study with steel powders ( $7.76\text{-}7.81\text{ g/cm}^3$ ) are almost identical to those of the corresponding wrought steels (around  $7.83\text{-}7.86\text{ g/cm}^3$ ) (ASM, 1961) and are much higher than densities of SLS specimens produced with a mixture of iron and graphite powders ( $7.127\text{ g/cm}^3$  by Murali et al. (2003),  $6.3\text{ g/cm}^3$  by Simchi and Pohl (2004), and  $7.3\text{ g/cm}^3$  by Rombouts et al. (2006)).

### **3.2. Pore formation**

In order to get insights into pore formation mechanisms, single- and double-line

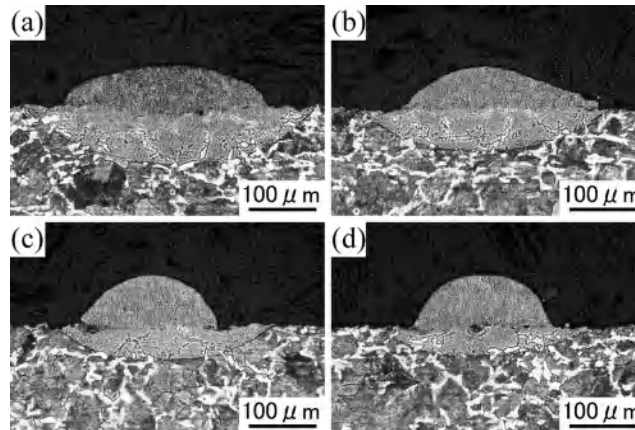


Fig. 4 Optical microstructures of single-line laser scan tracks formed with S75C powder on the flat substrate at various scan speeds of (a) 50 mm/s, (b) 100 mm/s, (c) 150 mm/s and (d) 200 mm/s. Observations were made in a cross-section cut perpendicular to the scan direction at the middle of the track length (8mm).

laser scan tracks formed with steel powders spread in a thickness of 50  $\mu\text{m}$  on the flat substrate (S50C) are inspected in detail. Figure 4 shows optical microstructures of single-line laser scan tracks formed with S75C powder on the flat substrate at various scan speeds in the range of 50-200 mm/s. Observations were made in a cross-section cut perpendicular to the scan direction at the middle of the track length (8mm). The specimens were immersed in an etchant of 3% nital prior to observations, in order to clearly distinguish the laser-beam affected zone on the laser scan track from the flat substrate. A protrusion is formed on the laser scan track with the size and shape depending on the laser scan speed. As the scan speed increases from 50 to 200 mm/s, the height of the protrusion obviously increases and its width decreases. When the scan

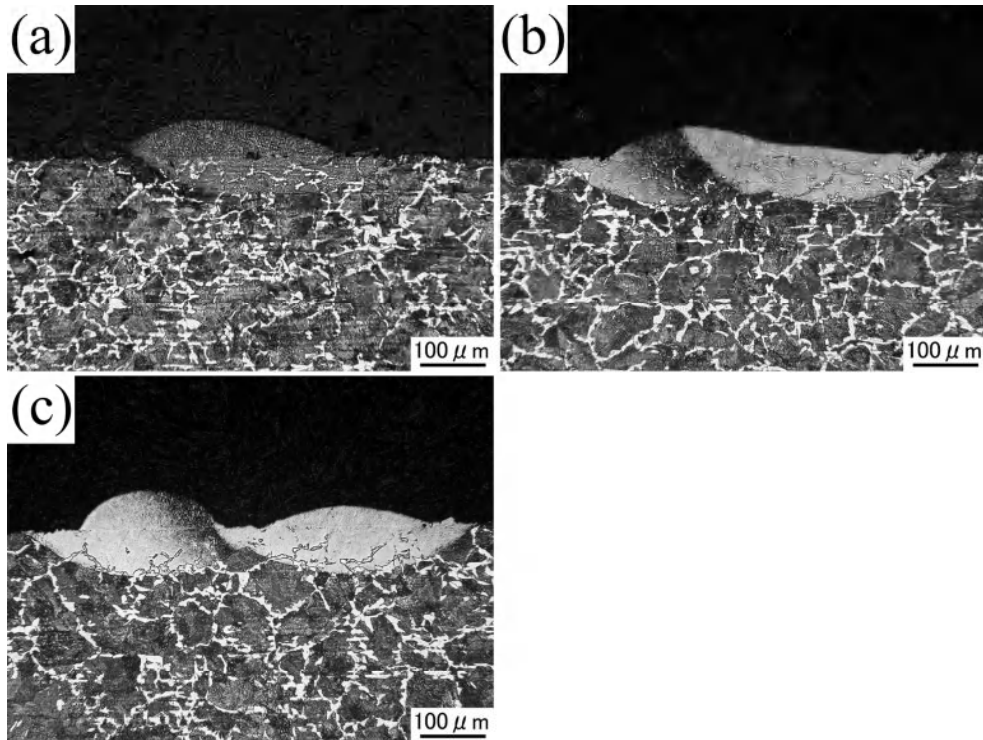


Fig. 5 Optical microstructures of double-line laser scan tracks formed with S75C powder on the flat substrate at various scan spacings of (a) 0.1 mm, (b) 0.2 mm and (c) 0.3 mm. The laser scan was made back and forth to draw a double-line track at a constant scan speed of 100 mm/s. Observations were made in a cross-section cut perpendicular to the scan direction at the middle of the track length (8mm).

speed exceeds 150 mm/s, the height of the protrusion is much larger than the powder spreading thickness ( $50\ \mu\text{m}$ ), causing the collision of the sintered specimen with the recoating blade during SLS processing, by which the processing is suspended.

Figure 5 shows optical microstructures of double-line laser scan tracks formed with S75C powder on the flat substrate at various scan spacings in the range of 0.1-0.3 mm. The laser scan was made back and forth to draw a double-line track at a constant

scan speed of 100 mm/s. As the scan spacing increases, the separation of protrusions formed on each of the double laser scan tracks becomes more evident. When the separation of protrusions is large, a large gap is formed between the protrusions. Powder filled in such gaps may not be easily sintered in the next scan, since the effective thickness of powder layer is significantly increased. Then, the corresponding portions remain pockets of non-sintered powders, which are essentially pores in the sintered body.

Figure 6 shows optical microstructures of double-line laser scan tracks formed with various steel powders on the flat substrate at the constant scan spacing of 0.2 mm and scan speed of 100 mm/s. As the carbon content in steel powders increases, the height of the protrusion obviously decreases and its width increases. As a result, the gap formed between the protrusions on the double laser scan tracks is larger as the carbon content in steel powders decreases. This is consistent with the present experimental result that the volume fraction of pores in SLS specimens increases as the carbon

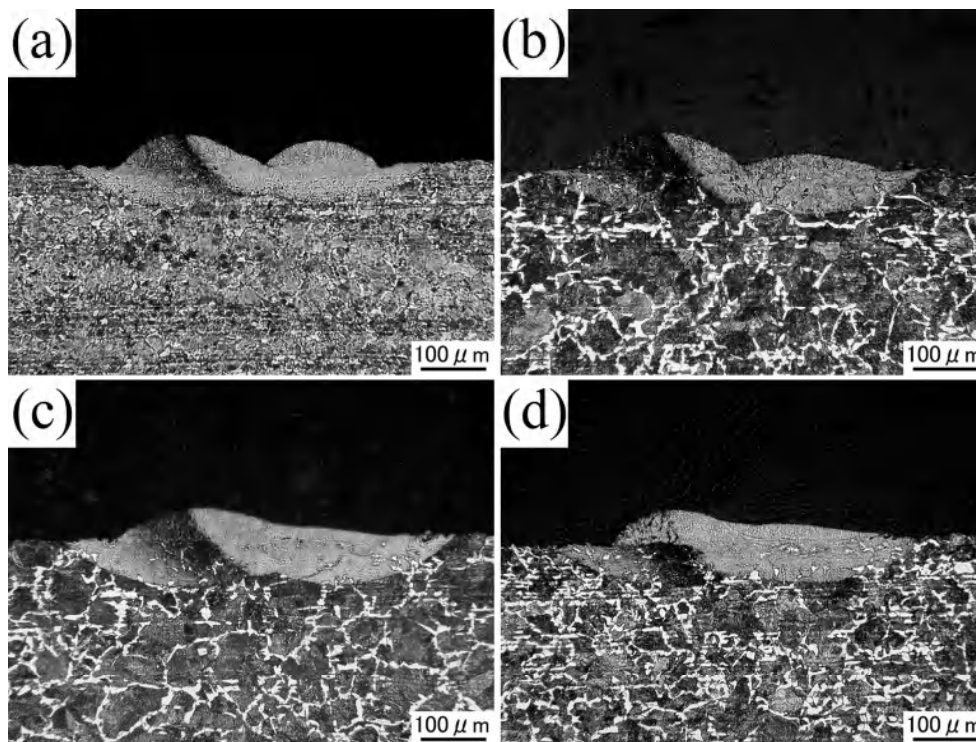


Fig. 6 Optical microstructures of double-line laser scan tracks formed with (a) S33C, (b) S50C, (c) S75C and (d) S105C powders on the flat substrate at the constant scan spacing of 0.2 mm and scan speed of 100 mm/s. The laser scan was made back and forth to draw a double-line track. Observations were made in a cross-section cut perpendicular to the scan direction at the middle of the track length (8mm).

content in steel powders decreases, as described in the 3.1. section. Plan views of single-line laser scan tracks formed with various steel powders on the flat substrate at a constant scan speed of 100 mm/s are illustrated in Fig. 7. The width of the scan track tends to increase as the carbon content in steel powder increases. While the scan track is continuous and smooth (less variation in height) at higher carbon contents (Figs. 7(c) and (d)), the smoothness of the track is significantly deteriorated at lower carbon contents (Figs. 7(a) and (b)). In addition to the surface roughness of the laser scan track, some droplets are observed to form in the vicinity of the track when the carbon content is low, indicating the high value of surface tension of molten Fe-C alloys when the carbon content is low. In fact, it is well known that the surface tension of molten Fe-C binary alloys decreases as the carbon content increases (Kozakevitch and Urbain, 1961; Tsarevskii and Popel', 1960). On top of that, the melting point of Fe-C binary alloys decreases as the carbon content increases up to 4.30 mass% (ASM, 1986). The wettability of molten Fe-C alloys is thus expected to be larger as the carbon content increases. This leads to the low volume fraction of pores in SLS specimens produced with high carbon steels.

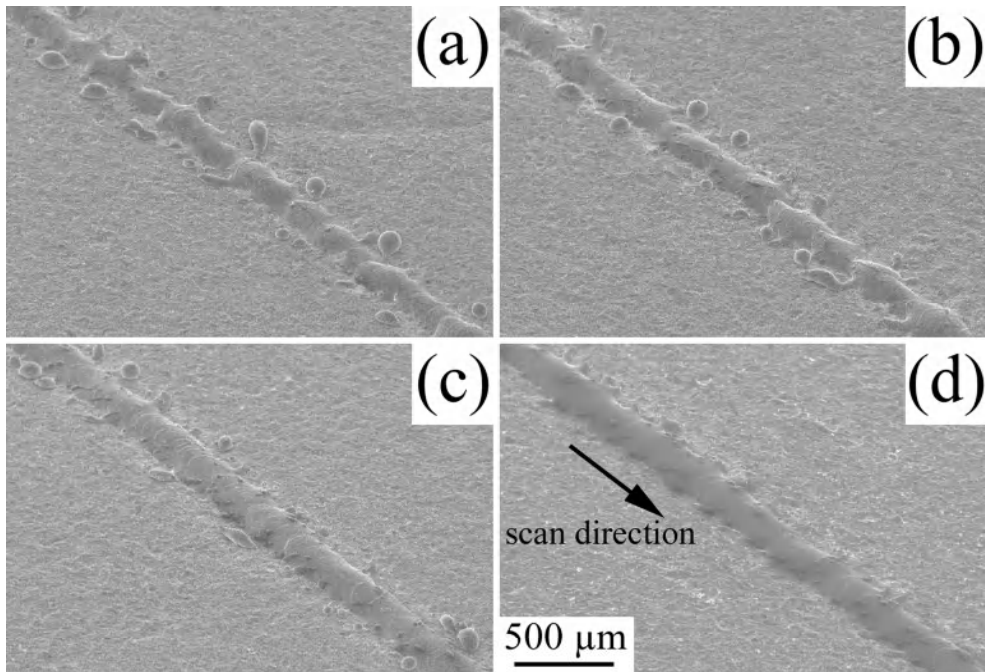


Fig. 7 Plan views of single-line laser scan tracks formed with (a) S33C, (b) S50C, (c) S75C and (d) S105C powders on the flat substrate at a constant scan speed of 100 mm/s.

### 3.3. Microstructure and mechanical property

#### 3.3.1. Effects of laser irradiation conditions

Optical microstructures in the surface and interior regions of a pore-free SLS specimen produced with S75C powder at the scan speed of 50 mm/s and scan spacing of 0.1 mm are shown in Figs. 8(a) and (b), respectively. Their magnified images are also shown respectively in Figs. 8(c) and (d). The building direction is parallel to the vertical edge of Fig. 8(a) and the surface region corresponds to the last few sintered layers. Accordingly, the microstructure observed in the surface region (Figs. 8(a) and (c)) is

quite different from that observed in the interior region (Figs. 8(b) and (d)). The surface region (200  $\mu\text{m}$  in depth) looks bright, indicating that the microstructure of the corresponding region is hardly etched with an etchant of 3% nital. The microstructure of the surface region is revealed to consist of a homogeneous martensite structure after etching with an etchant of hydrochloric picral (Fig. 8(e)). The martensitic structure in the surface region is considered to form as a result of rapid cooling of the last few sintered layers. On the other hand, the microstructure in the interior region consists of a fine pearlite structure (a mixture of sorbite and troostite) (Fig. 8(d)). The fine pearlite structure observed in the interior region is considered to form as a result of tempering (transformation) of the microstructure observed in the surface region, which occurs during the SLS process. The average value of microhardness of the surface area is 816 HV, which is much higher than that (418 HV) obtained in the interior region.

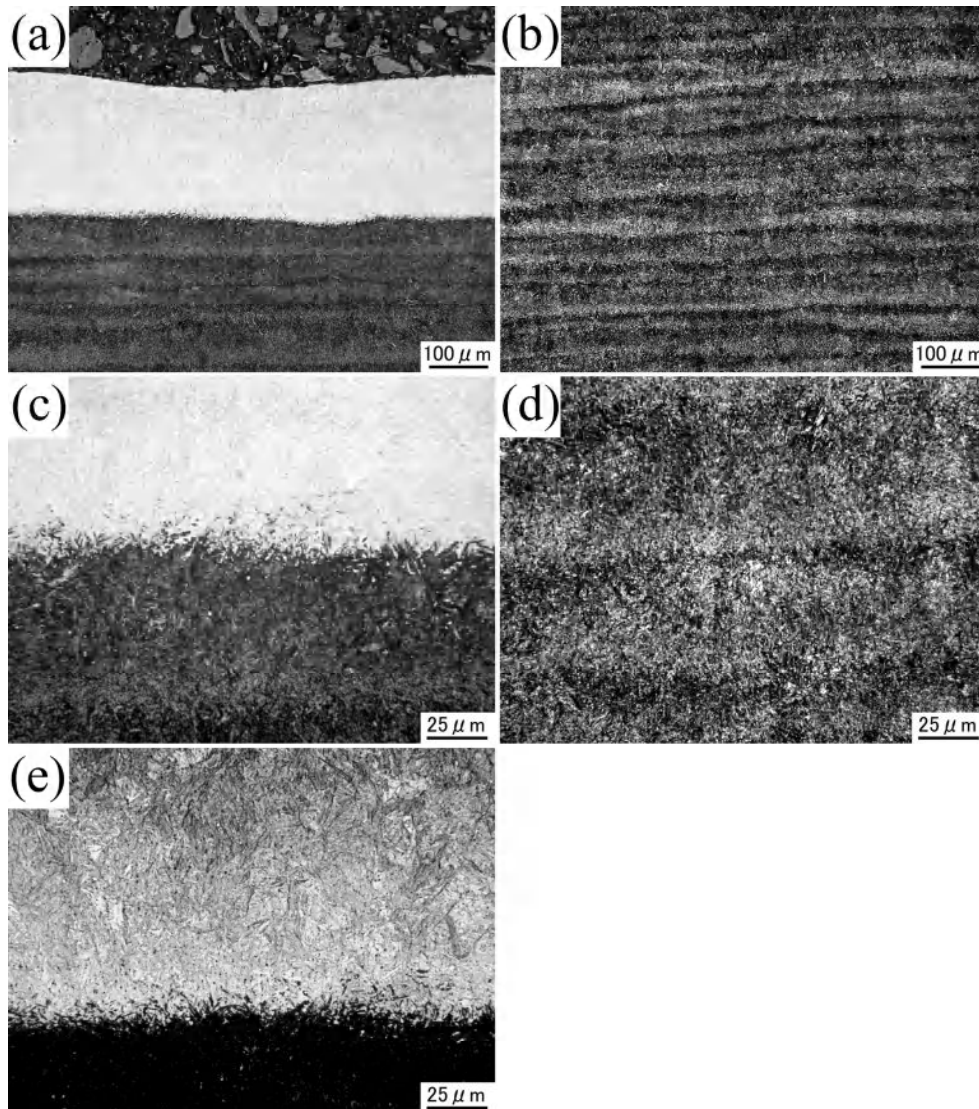


Fig. 8 Optical microstructures in the surface and the interior regions of a pore-free SLS specimen produced under the same condition of Fig. 1(d) (scan speed of 50 mm/s and scan spacing of 0.1 mm) using S75C powder. Magnified images from the surface ((a)) and the interior ((b)) regions are shown in (c) and (d), respectively. Optical microstructure in the surface region of Fig. 8(c) after immersing the specimen in an etchant of hydrochloric picral is shown in (e).

Optical microstructures in the interior region of almost pore-free SLS specimens produced with S75C powder at various laser irradiation conditions are shown in Fig. 9.

The irradiation conditions employed for Figs. 9(a), (b), (c) and (d) are exactly the same as those used for producing the almost pore-free specimens of Figs. 1(d), (c), (b) and (h), respectively. While the SLS specimens of Figs. 9(a) and (b) exhibit a microstructure consisting of a mixture of sorbite and troostite, the SLS specimen of Fig. 9(c) exhibits a troostite microstructure. When considering the fact that the total energy input during the SLS process decreases as the scan spacing increases, the formation of troostite microstructure in the SLS specimen produced at the scan speed of 50 mm/s and scan spacing of 0.3 mm (Fig. 9(c)) is considered to be due to the fact that the tempering temperature and time the SLS specimen of Fig. 9(c) experienced are respectively a little lower and shorter than those the SLS specimens produced at the scan speed of 50 mm/s and scan spacings of 0.1 and 0.2 mm (Figs. 9(a) and (b)) experienced. The microstructure of the SLS specimen produced at the scan speed of 50 mm/s and scan spacing of 0.2 mm (Fig. 9(b)) is very similar to that produced at the scan speed of 100 mm/s and scan spacing of 0.1 mm (Fig. 9(d)). This is reasonable, since the total energy inputs during the SLS process for these two specimens are identical with each other. The average value of microhardness of the interior regions and the yield stress defined as the 0.2% offset stress in compression tests for these SLS specimens are tabulated in Table 3. The tendency observed for the microhardness and yield stress is consistent with

the observed variation in microstructures. The values of microhardness and yield stress tend to be higher for specimens produced with a lower energy input. This clearly indicates that in order to achieve high strength for SLS parts, the energy density employed for SLS processing of high carbon steels should be chosen not to exceed much the critical value for full densification.

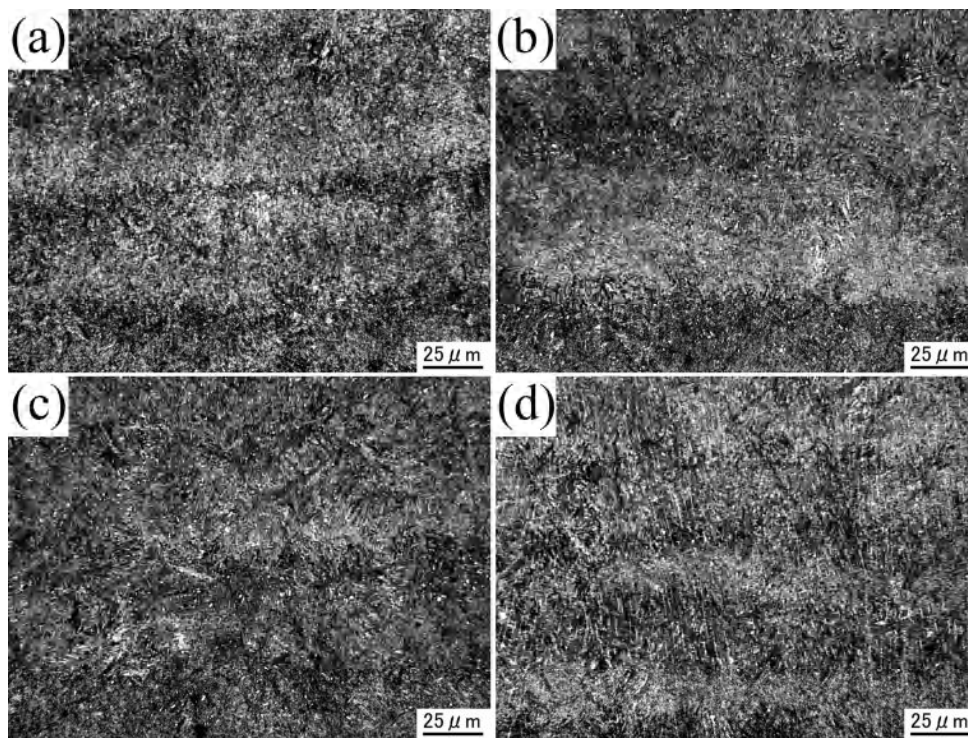


Fig. 9 Optical microstructures in the interior region of almost pore-free SLS specimens produced with S75C powder at various laser irradiation conditions with the scan speed/scan spacing of (a) 50 mm/s, 0.1 mm, (b) 50 mm/s, 0.2 mm, (c) 50 mm/s, 0.3 mm and (d) 100 mm/s, 0.1 mm, respectively.

Table 3 Average value of microhardness and yield stress of the interior regions of SLS specimens produced with the same conditions as Fig. 9

Sample	Scan speed (mm/s)	Scan spacing (mm)	Yield stress (MPa)	Hardness (HV(4.9N))
a	50	0.1	1153	418
b	50	0.2	1188	454
c	50	0.3	1273	484
d	100	0.1	1163	451

### 3.3.2. Effects of carbon contents

Optical microstructures in the surface and interior regions of pore-free SLS specimens produced with S50C, S75C and S105C powders under the same laser irradiation condition used for Fig. 1(d) (scan speed of 50 mm/s and scan spacing of 0.1 mm) are shown in Fig. 10. While the interior regions of all the SLS specimens exhibit a homogeneous and fine pearlite microstructure (Figs. 10(d), (e) and (f)), the microstructure in the surface regions differ from specimen to specimen. While the surface region of the SLS specimen produced with S75C powder exhibit a homogeneous martensite microstructure (Fig. 10(b)), that produced with S105C powder exhibits a microstructure consisting of martensite and retained austenite (Fig. 10(c)). On the other hand, the surface region of the SLS specimen produced with S50C powder exhibits a microstructure consisting of martensite and very fine pearlite (nodular troostite) (Fig. 10(a)).

The yield stress and microhardness values in the interior regions of these pore-free

SLS specimens are plotted in Fig. 11 as a function of carbon content in steel powders. The values of yield stress and microhardness tend to increase as the carbon content in steel powders increases. To be noted in Fig. 11 is that the values of both yield stress and microhardness of the SLS specimens produced by S75C powder are considerably larger than those of the corresponding wrought steel subjected to tempering at 650°C (Monma, 1981). This is believed to arise from the formation of fine microstructures by rapid cooling from the melt during the SLS process.

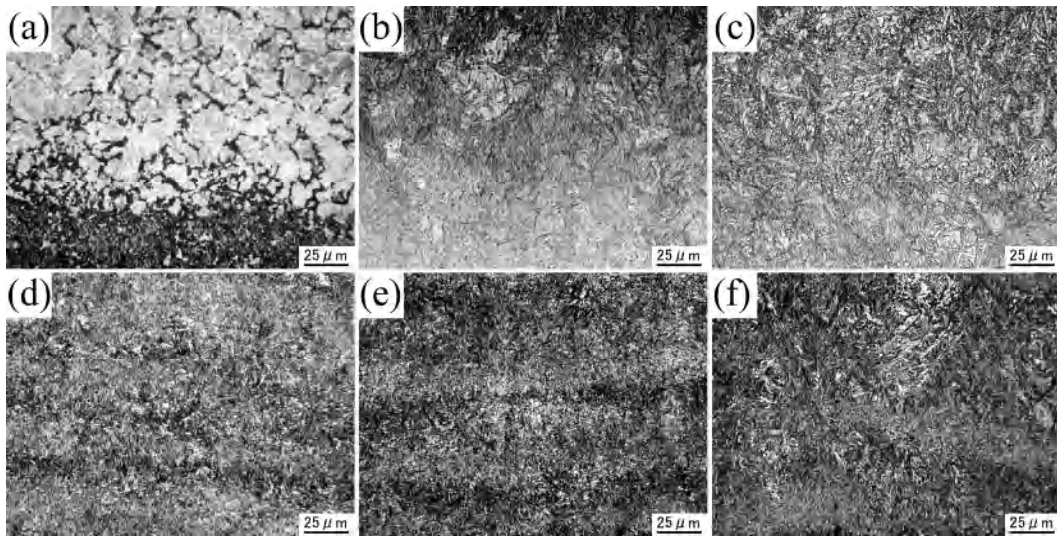


Fig. 10 Optical microstructures in the surface ((a), (b), (c)) and interior ((d), (e), (f)) regions of pore-free SLS specimens produced with S50C ((a), (d)), S75C ((b), (e)) and S105C ((c), (f)) powders under the same laser irradiation condition used for Fig. 1(d) (scan speed of 50 mm/s and scan spacing of 0.1 mm).

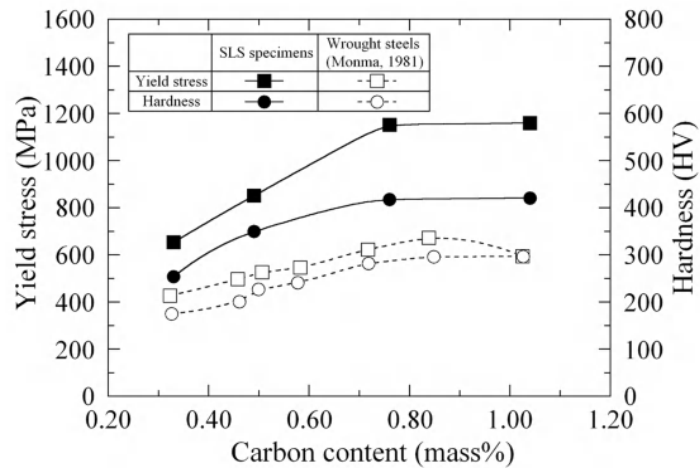


Fig. 11 Yield stress and microhardness in the interior regions of each of pore-free SLS specimens produced at the scan speed of 50 mm/s and scan spacing of 0.1 mm plotted as a function of carbon content in steel powders.

#### 4. Conclusion

Optimum conditions for laser irradiation to achieve fully dense high carbon steel SLS (Selective Laser Sintering) specimens have been investigated as a function of carbon content in steel powders with the use of steel powders with different carbon contents in the range of 0.33-1.05 mass%C. The results obtained are summarized as follows.

- (1) The volume fraction of pores in carbon steels produced by the SLS process decreases as the scan speed and scan spacing decrease. The increase in the carbon content in carbon steel powders can effectively decrease the volume fraction of pores in the specimens produced by the SLS process.

(2) Once the energy input during the SLS process is sufficiently large, full densification with the density comparable to those of the corresponding wrought steels is easily achieved. The energy density during the SLS process required for full densification decreases as the carbon content increases from 400 J/mm<sup>3</sup> for 0.33 and 0.50 mass%C to 267 J/mm<sup>3</sup> for 0.75 and 1.05 mass%C, because of the increased wettability of molten Fe-C alloys for the higher carbon contents.

(3) The values of microhardness and yield stress of fully dense SLS specimens tend to increase as the carbon content in steel powders increases. At a given carbon content, the values of microhardness and yield stress of fully dense SLS specimens tend to be higher for those produced with a lower energy input (with higher laser scan speeds and larger scan spacings), indicating that the energy density employed for SLS processing of high carbon steels should be chosen not to exceed much the critical value for full densification for high strength.

### **Acknowledgements**

This work was supported by JST, Research for Promoting Technological Seeds Project through the project No. 11-078, 2008.

### **References**

- Abe, F., Osakada, K., Shiomi, M., Uematsu, K., Matsumoto, M., 2001. The manufacturing of hard tools from metallic powders by selective laser melting. *J. Mater. Process. Technol.* 111, 210-213.
- Abe, S., Higashi, Y., Fuwa, I., Yoshida, N., Yoneyama, T., 2006. Milling-combined laser metal sintering system and production of injection molds with sophisticated functions. In: *Proceedings of the 11th International Conference on Precision Engineering (ICPE)*, Tokyo, Japan, pp. 285-290.
- ASM Committee on Constitution of Binary Alloys, 1986. Fe-C phase diagram. In: *Massalski, T.B., Murray, J.L., Bennett, L.H., Baker, H. (Eds.), Binary Alloy Phase Diagrams*, vol. 1. ASM, Metals Park, Ohio, p. 562.
- ASM Metals Handbook Committee, 1961. Density of metals and alloys. In: *Lyman, T. (Ed.), Metals Handbook*, 8th ed., vol. 1. ASM, Metals Park, Ohio, p. 52.
- Kozakevitch, P., Urbain, G., 1961. *Mém. Sci. Rev. Mét.* 58, 931.
- Kruth, J.P., Wang, X., Laoui, T., Froyen, L., 2001. Progress in selective laser sintering. In: *Proceedings of the 13th International Symposium for Electromachining (ISEM-XIII)*, Bilbao, Spain, vol II, pp. 21-38.
- Levy, G.N., Schindel, R., Kruth, J.P., 2003. Rapid manufacturing and rapid tooling with layer manufacturing (LM) technologies, state of the art and future perspectives.

- Annals of the CIRP 52 (2), 589-609.
- Monma, K., 1981. Tekkozairyogaku. Zikkyo Shuppan, Tokyo, p. 179 (in Japanese).
- Murali, K., Chatterjee, A.N., Saha, P., Palai, R., Kumar, S., Roy, S.K., Mishra, P.K., Choudhury, A.R., 2003. Direct selective laser sintering of iron–graphite powder mixture. *J. Mater. Process. Technol.* 136, 179-185.
- Nakamoto, T., Shirakawa, N., Miyata, Y., Sone, T., Inui, H., 2008. Selective laser sintering and subsequent gas nitrocarburizing of low carbon steel powder. *Int. J. of Automation Technology* 2 (3), 168-174.
- Niu, H.J., Chang, I.T.H., 1998. Liquid phase sintering of M3/2 high speed steel by selective laser sintering. *Scripta Mater.* 39 (1), 67-72.
- ÓDonnchadha, B., Tansey, A., 2004. A note on rapid metal composite tooling by selective laser sintering. *J. Mater. Process. Technol.* 153-154, 28-34.
- Otsu, M., Fukunaga, T., Uemura, M., Takemasu, T., Miura, H., 2005. Laser sintering of low alloy and tool steel powders. In: *Proceedings of the 2nd JSME/ASME International Conference on Materials and Processing*, (APP-02) pp. 1-4.
- Rombouts, M., Kruth, J.P., Froyen, L., Mercelis, P., 2006. Fundamentals of selective laser melting of alloyed steel powders. *CIRP Annals* 55 (1), 187-192.
- Simchi, A., Asgharzadeh, H., 2004. Densification and microstructural evaluation during

laser sintering of M2 high speed steel powder. *Mater. Sci. Technol.* 20, 1462-1468.

Simchi, A., Pohl, H. 2003. Effects of laser sintering processing parameters on the microstructure and densification of iron powder. *Mater. Sci. Eng. A* 359, 119-128.

Simchi, A., Pohl, H., 2004. Direct laser sintering of iron–graphite powder mixture. *Mater. Sci. Eng. A* 383, 191-200.

Tsarevskii, B.V., Popel', S.I., 1960. *Izv. VUZov. Cher. Met.* No. 8, 15.

## Figure captions

Fig. 1 Optical microstructures of SLS specimens produced with S75C steel powder under various laser irradiation conditions with the scan speed/scan spacing of (a) 50 mm/s, 0.4 mm, (b) 50 mm/s, 0.3 mm, (c) 50 mm/s, 0.2 mm, (d) 50 mm/s, 0.1 mm, (e) 100 mm/s, 0.4 mm, (f) 100 mm/s, 0.3 mm, (g) 100 mm/s, 0.2 mm and (h) 100 mm/s, 0.1 mm, respectively. Observations were made in a cross-section cut parallel to the building direction.

Fig. 2 Energy density required for full densification by SLS processing plotted as a function of carbon content in steel powders.

Fig. 3 Optical microstructures of SLS specimens produced with (a) S33C, (b) S50C, (c) S75C and (d) S105C steel powders at the scan speed of 100 mm/s and scan spacing of 0.2 mm. Observations were made in a cross-section cut parallel to the building direction.

Fig. 4 Optical microstructures of single-line laser scan tracks formed with S75C powder on the flat substrate at various scan speeds of (a) 50 mm/s, (b) 100 mm/s, (c) 150

mm/s and (d) 200 mm/s. Observations were made in a cross-section cut perpendicular to the scan direction at the middle of the track length (8mm).

Fig. 5 Optical microstructures of double-line laser scan tracks formed with S75C powder on the flat substrate at various scan spacings of (a) 0.1 mm, (b) 0.2 mm and (c) 0.3 mm. The laser scan was made back and forth to draw a double-line track at a constant scan speed of 100 mm/s. Observations were made in a cross-section cut perpendicular to the scan direction at the middle of the track length (8mm).

Fig. 6 Optical microstructures of double-line laser scan tracks formed with (a) S33C, (b) S50C, (c) S75C and (d) S105C powders on the flat substrate at the constant scan spacing of 0.2 mm and scan speed of 100 mm/s. The laser scan was made back and forth to draw a double-line track. Observations were made in a cross-section cut perpendicular to the scan direction at the middle of the track length (8mm).

Fig. 7 Plan views of single-line laser scan tracks formed with (a) S33C, (b) S50C, (c) S75C and (d) S105C powders on the flat substrate at a constant scan speed of

100 mm/s.

Fig. 8 Optical microstructures in the surface and the interior regions of a pore-free SLS specimen produced under the same condition of Fig. 1(d) (scan speed of 50 mm/s and scan spacing of 0.1 mm) using S75C powder. Magnified images from the surface ((a)) and the interior ((b)) regions are shown in (c) and (d), respectively. Optical microstructure in the surface region of Fig. 8(c) after immersing the specimen in an etchant of hydrochloric picral is shown in (e).

Fig. 9 Optical microstructures in the interior region of almost pore-free SLS specimens produced with S75C powder at various laser irradiation conditions with the scan speed/scan spacing of (a) 50 mm/s, 0.1 mm, (b) 50 mm/s, 0.2 mm, (c) 50 mm/s, 0.3 mm and (d) 100 mm/s, 0.1 mm, respectively.

Fig. 10 Optical microstructures in the surface ((a), (b), (c)) and interior ((d), (e), (f)) regions of pore-free SLS specimens produced with S50C ((a), (d)), S75C ((b), (e)) and S105C ((c), (f)) powders under the same laser irradiation condition used for Fig. 1(d) (scan speed of 50 mm/s and scan spacing of 0.1 mm).

Fig. 11 Yield stress and microhardness in the interior regions of each of pore-free SLS specimens produced at the scan speed of 50 mm/s and scan spacing of 0.1 mm plotted as a function of carbon content in steel powders.

### **Table captions**

Table 1 Chemical composition of carbon steel powders (mass%). Numbers in ( ) indicate the carbon contents after SLS processing.

Table 2 Laser irradiation conditions

Table 3 Average value of microhardness and yield stress of the interior regions of SLS specimens produced with the same conditions as Fig. 9